ACS OMEGA

Article

Cite This: ACS Omega 2019, 4, 185−194

http://pubs.acs.org/journal/acsodf

Improved High Temperature Performance of a Spinel $LiNi_{0.5}Mn_{1.5}O_4$ Cathode for High-Voltage Lithium-Ion Batteries by Surface Modification of a Flexible Conductive Nanolayer

Hongyu Dong,[†,‡,§] Yijia Zhang,[†,‡,§] Shiquan Zhang,[†,‡,§] Panpan Tang,[†,‡,§] Xinglu Xiao,[†,‡,§] Mengyue Ma,[§,∥] Huishuang Zhang,[†,‡,§] Yanhong Yin,[†,‡,§] Dong Wang,*[,†,‡] and Shuting Yang*[,†,‡,§]

[†]College of Chemistry and Chemical Engineering, [‡]National & Local Engineering Laboratory for Motive Power and Key Materials, [§]Collaborative Innovation Center of Henan Province for Motive Power and Key Materials, and [∥]Henan Battery Research Institute, Henan Normal University, Construction East Road, Xinxiang, Henan 453007, P. R. China

ABSTRACT: The composite cathode material of the conductive polymer polyaniline (PANI)-coated spinel structural $LiNi_{0.5}Mn_{1.5}O_4$ (LNMO) for high-voltage lithium-ion batteries has been successfully synthesized by an in situ chemical oxidation polymerization method. The electrode of the LNMO−PANI composite material shows superior rate capability and excellent cycling stability. A capacity of 123.4 mAh g^{-1} with the capacity retention of 99.7% can be maintained at 0.5C after 200 cycles in the voltage range of 3.0−4.95 V (vs Li/Li^+) at room temperature. Even with cycling at 5C, a capacity of 65.5 mAh g^{-1} can still be achieved. The PANI coating layer can not only reduce the dissolution of Ni and Mn from the LNMO cubic framework into the electrolyte during cycling, but also significantly improve the undesirable interfacial reactions between the cathode and electrolyte, and markedly increase the electrical conductivity of the electrode. At 55 °C, the LNMO−PANI composite material exhibits more superior cyclic performance than pristine, that is, the capacity retention of 94.5% at 0.5C after 100 cycles vs that of 13.0%. This study offers an effective strategy for suppressing the decomposition of an electrolyte under the highly oxidizing (>4.5 V) and elevated temperature conditions.

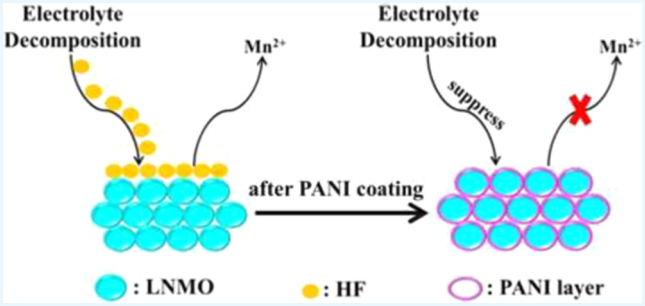

INTRODUCTION

Compared to anode materials, cathode materials exhibit a relatively lower specific capacity and hardly meet the increasing energy needs.[1,2] It is significant for lithium-ion batteries to increase their working voltage to achieve the energy demands.[3] Whereupon, $LiNi_{0.5}Mn_{1.5}O_4$ (LNMO) has been considered as one of the most promising cathodes for lithium-ion batteries due to low-cost and pollution-free nature.[4−8] In particular, it also attains a high-energy density of 686 Wh kg^{-1} by the redox couples of Ni^{2+}/Ni^{4+} located at ∼4.7 V (vs Li/Li^+) in the spinel LNMO.[9]

In terms of these great superiorities, LNMO is paid more and more attention by scientific research workers. However, its self-deficiencies still exist which may obstruct its further development.[10] Primarily, the pivotal voltage platform of LNMO (∼4.7 V vs Li/Li^+) beyond the stabilized limitation of the traditional electrolyte (≤4.5 V vs Li/Li^+) cannot effectively resist the oxidation decomposition of the electrolyte under such high electric potential.[11] This may lead to the generation of a pernicious solid electrolyte interphase film which could hinder the intercalation/deintercalation for lithium ions and increase the interface resistance.[12,13] Furthermore, it may cause Ni and Mn atoms to dissolve from the spinel LNMO spinel into the electrolyte due to HF, as well as the Ni and Mn ions dissolution may be accelerated under high temperature and pressure.[14−18] The equations are as follows

$$LiPF_6 + 4H_2O \rightarrow LiF + PO_4H_3 + 5HF \quad (1)$$

$$DEC + LiPF_6 \rightarrow C_2H_5OCOOPF_4 + C_2H_4 + HF + LiF \quad (2)$$

$$2LNMO + 4H^+ + 4F^- \rightarrow 3Ni_{0.25}Mn_{0.75}O_2 + 0.25NiF_2 + 0.75MnF_2 + 2LiF + 2H_2O \quad (3)$$

Finally, the Jahn−Teller distortion also propels the Mn^{3+} ions to form Mn^{2+} in the further stage of discharge cycling[19] and the Mn^{2+} ions squint towards to dissolve into the electrolyte, resulting in the irreversible capacity loss. In particular, detrimental reactions may be expedited at elevated temperatures,[20] and it immensely obstructs the commercialized prospect of the high-voltage LNMO cathode for lithium-ion batteries.

Received: September 28, 2018
Accepted: December 26, 2018
Published: January 4, 2019

DOI: 10.1021/acsomega.8b02571
ACS Omega 2019, 4, 185−194

Universally, it is proved that surface coating using some metal oxides is an appropriate strategy to surmount these deficiencies of LNMO, such as Al_2O_3,[21] ZnO,[22,23] TiO_2,[24] Fe_2O_3,[25] $LaFeO_3$,[1818] Li_2SiO_3,[26] Li_2SnO_3,[27] $LiCoO_2$,[17] etc. The results show that these metal oxides, working as a protective layer, could avoid the undesirable interface reactions and reduce the dissolution amounts of the transition metal ions. To a certain extent, these coating layers have improved the LMNO material performance. Meanwhile, another approach has been utilized to ameliorate the cycling stability of the LNMO electrode with carbon coating.[28−31] But it is possible for the high valence of Mn and Ni in LNMO to revert to the low state during carbonizing at high temperature. Accordingly, it is urgent to discover a new kind of coating agent which can not only act as a protective skin but also can enhance the electrical conductivity.

Since the conductive polymers were regarded as a superior coating agent, they are favorable materials coated on LMNO to improve cycling stabilities at room and elevated temperatures. For instance, Kim et al.[32] have studied that polyimide (PI) was coated on the surface of LNMO by thermal polymerization, and it could optimize the unwanted interfacial reactions and provide the superior lithium storage properties by the introduction of the PI coating layer. However, the low cycle ability of the LNMO−PI composite electrode under elevated temperatures was attributed to the poor compatibility toward the electrolyte solution. Subsequently, Gao et al.[33] have reported that a polypyrrole was used to coat on the LNMO surface via a chemical oxidation polymerization method. In spite of the great improvement of the conductivity, the lithium storage capacity is still not very ideal. Hence, it is still meaningful to seek another conductive polymer to improve electrochemical performance of LNMO on the basis of good conductivity. In the field of conductive polymers, polyaniline (PANI) has been paid close attention because of the cheap raw materials and easy preparation process.[34−38] In this study, we have successfully prepared the PANI-coated LNMO electrode by a simple in situ chemical oxidative polymerization method in the ice-water bath. As expected, LNMO−PANI composite material shows superior rate capability and excellent cycling stability. A capacity of 123.4 mAh g^{-1} with the capacity retention of 99.7% can be maintained at 0.5C after 200 cycles in the voltage range of 3.0−4.95 V (vs Li/Li^+) at room temperature. Even with cycling at 5C, a capacity of 65.5 mAh g^{-1} can still be achieved. The PANI coating layer can not only reduce the dissolution of Ni and Mn from the LNMO cubic framework into the electrolyte during cycling, but also significantly improve the undesirable interfacial reactions between the cathode and the electrolyte, and markedly increase the electrical conductivity of the electrode.

RESULTS AND DISCUSSION

From Figure 1, the presence of PANI in the composite was confirmed by the Raman spectrometer. The bare LNMO exhibits that the stretching vibration of Mn−O in the MnO_6 octahedral phase is located at 634 cm^{-1}. The characteristic bands of 402 and 494 cm^{-1} are corresponding to the stretching vibrations of Ni−O, and the characteristic band of 598 cm^{-1} is in accordance with the T_{2g} vibration mode of the spinel structural compounds.[39,40] Beyond this, there also appears the characteristic bands of polyaniline in the as-prepared LNMO−PANI composite material. The characteristic bands at 1550 and 1453 cm^{-1} may be the stretching vibration of C═C and

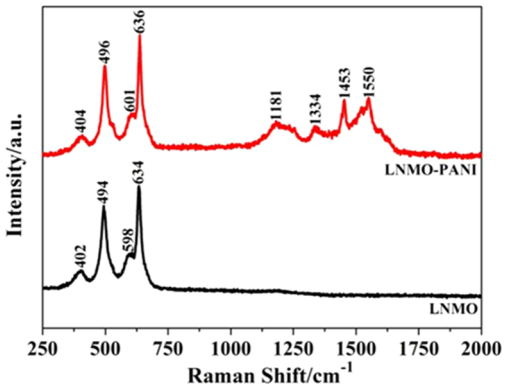

Figure 1. Raman patterns of the bare LNMO and the LNMO−PANI composite material.

C═N in the quinoid (−N═Q═N−, where Q = quinoid frame) model. The characteristic band of 1334 cm^{-1} is assigned to the stretching vibration of C−N in the benzenoid unit. The characteristic band at 1181 cm^{-1} belongs to the stretching vibration of the quinoid model. The appearance of these iconic characteristic bands proves the presence of PANI in the synthesized composite.[41,42]

The PANI content in the composite was determined by thermogravimetric analysis (TGA) in Figure 2. The samples

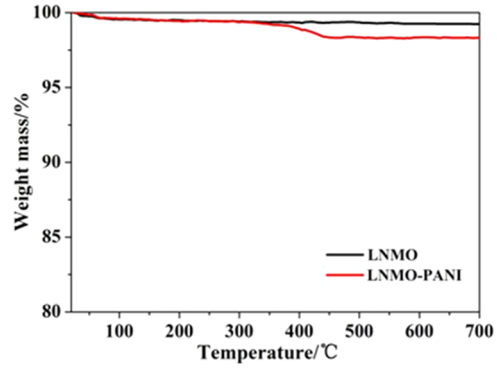

Figure 2. Thermogravimetric analysis (TGA) image of the bare LNMO and the LNMO−PANI composite material.

were heated from 20 to 700 °C at a rate of 10 °C min^{-1} under air atmosphere. It can be seen that the bare LNMO maintains a constant weight, however, the retained mass of the composite decreases as the temperature increases.[43] Therefore, it indicates that the PANI content in the composite is calculated to be about 1 wt %.

The morphologies of the bare LNMO and the LNMO−PANI composite material were characterized by field emission-scanning electron microscopy (FE-SEM) and transmission electron microscopy (TEM) as shown in Figure 3. A smooth surface of the bare LNMO can be seen in Figure 3a. However, a reversely rough surface of the LNMO−PANI composite material is observed in Figure 3b, which indicates that a relatively homogeneous PANI layer has been coated successfully on the surface of LNMO particles. As shown in Figure 3c, it is relatively well-distributed on the surface of the LNMO particles, and the thickness of the PANI layer is around 20 nm as shown in Figure 3d.

To further verify the dispersing of the coated PANI on the surface of the composite particles, energy dispersive spectros-

DOI: 10.1021/acsomega.8b02571
ACS Omega 2019, 4, 185−194

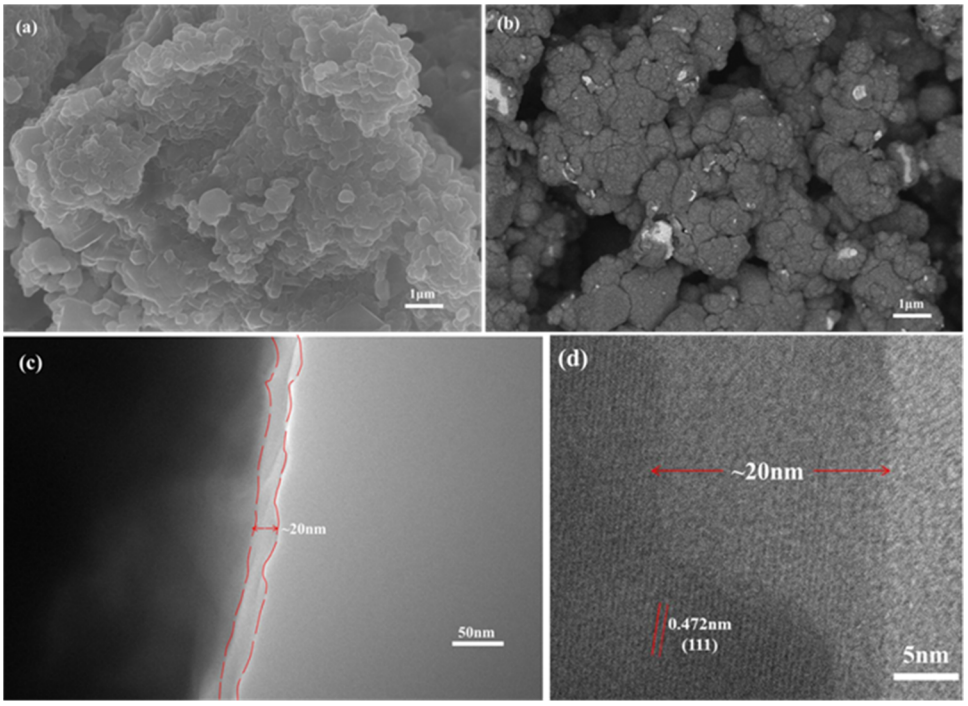

Figure 3. Field emission-scanning electron microscopy (FE-SEM) pictures of (a) the bare LNMO, (b) the LNMO−PANI composite material, the transmission electron microscopy (TEM) images of (c) coated on the outer surface of the LNMO particles and (d) thickness of the PANI layer of the LNMO−PANI composite material.

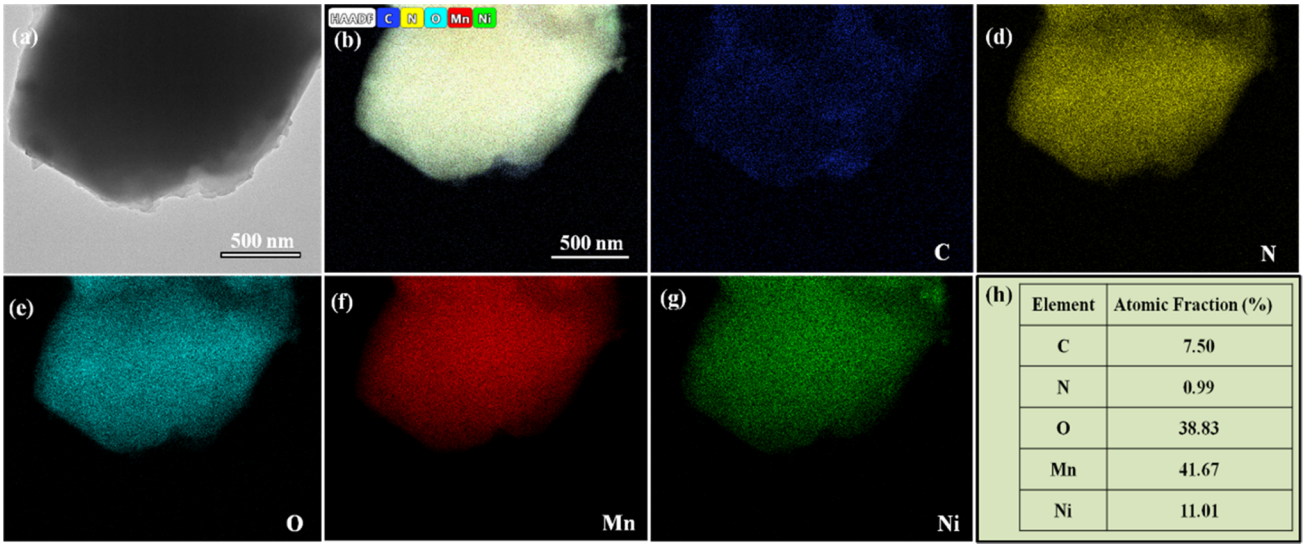

Figure 4. (a) High-angle annular dark field-scanning transmission electron microscopy image of the LNMO−PANI composite, (b-g) the EDS mappings of the TEM pattern for the LNMO−PANI composite material, (h) the atomic fraction of C, N, O, Mn, and Ni elements.

copy (EDS) of the TEM pattern was performed. From Figure 4a−g, it can be clearly observed that the disperse positions of the elements C and N are consistent with the distributed positions of the elements Ni, Mn, and O in the mappings. This confirms that the PANI layer uniformly coated on the surface of the LNMO particles again, and the atomic fraction is 0.99%, which is very close to the actual coating amount of PANI.

The X-ray diffraction (XRD) pattern of the bare LNMO and the LNMO−PANI composite material is displayed in Figure 5. It is demonstrated that the bare LNMO and LNMO−PANI composite material are both corresponding to the *Fd*3*m* cubic spinel structure (JCPDS No. 32-0581), and the PANI coating layer of the LNMO−PANI composite does not have obvious effect on the crystal crystallinity of the spinel LNMO.

The first, 100th, and 200th charge−discharge curves and cyclic voltammetry (CV) curves of the bare LNMO and LNMO−PANI composite material electrodes were obtained in the voltage range from 3.0 to 4.95 V (vs Li/Li^+) at room temperature (25 °C) as shown in Figure 6. The electrodes were first activated at 0.1C rate (1C = 147 mAh g^{-1}) for 3 cycles, and then they were tested at 0.5C for 200 cycles. In Figure 6a,b, there is a remarkable voltage plateau at ~4.7 V. This may be assigned to the Fermi level from Ni^{2+} to Ni^{4+}, which is confined to the top of the O 2p valence band,[44] and it

DOI: 10.1021/acsomega.8b02571
ACS Omega 2019, 4, 185−194

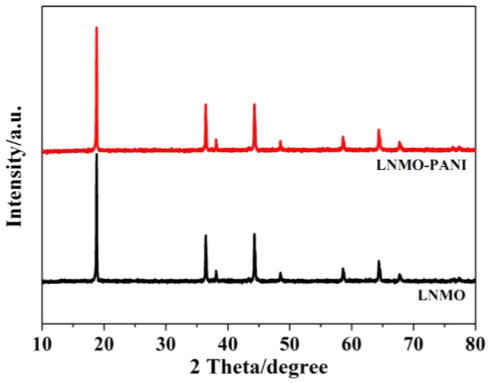

Figure 5. X-ray diffraction (XRD) pattern of the bare LNMO and the LNMO−PANI composite material.

can be ascribed to the two redox couples for Ni^{2+}/Ni^{3+} and Ni^{3+}/Ni^{4+} both located near 4.7 V. Whereupon, the voltage difference is specially wispy. In addition, there is also a tiny voltage plateau at ∼4.0 V in Figure 6a,b, which is associated with the Mn^{3+}/Mn^{4+} redox reaction. Compared with Figure 6a, the LNMO−PANI composite material electrode presents an excellent reversibility, and no other voltage plateaus are sighted in Figure 6b, indicating that the PANI does not lead to an extra redox reaction in the tested voltage range. It means that the PANI only remains stable during cycling and does not contribute to the discharge capacity. Figure 6c,d shows the cyclic voltammetry (CV) curves of the bare LNMO and the LNMO−PANI composite material electrodes at room temperature by a sweep rate of 0.05 mV s^{-1}. The two chief peaks located at around 4.7 V are attached to Ni^{2+}/Ni^{3+} and Ni^{3+}/Ni^{4+}, and the secondary peak at around 4.0 V is connected to the transformation of Mn^{3+}/Mn^{4+}. The peak area at ∼4.0 V is much smaller than the peak area at ∼4.7 V, which tautologically proves that the primary contribution to the discharge capacity is from the Ni^{2+}/Ni^{4+} redox couple. The over-potentials of the bare LNMO and the LNMO−PANI composite material electrodes are synchronized with 0.442 and 0.314 V during the first cycle, which means a much lower polarization during the electrochemical reaction process for the coated LNMO electrode. In addition, there is no additional peak after coating as shown in Figure 6c. It also indicates that the PANI does not practically involve in the redox reactions in the tested voltage range. The results discussed above are in great agreement with the consequence of the charge−discharge curves.[33]

The cycling and rate performances of the bare LNMO and the LNMO−PANI composite material at room temperature are shown in Figure 7. First, the cells were activated at 0.1C for 3 cycles, and then they were charged−discharged at 0.5C for 200 cycles in Figure 7a. The initial discharge capacity of the bare LNMO is 117.4 mAh g^{-1} at the first cycle, and then it increases and remains at about 120 mAh g^{-1} by 90 cycles. Afterwards, it continuously decreases to 115.4 mAh g^{-1} after 200 cycles. In contrast, the composite electrode exhibits a higher initial discharge capacity of 123.8 mAh g^{-1}, and after over 200 cycles, it is still remains at 123.4 mAh g^{-1}. The reversible capacity retention is as high as 99.7%. It is significant to find that the discharge specific capacity has achieved universal enhancement after PANI coating, which may be due to the polyaniline, which works as a valid protective layer and could effectively reduce the dissolution of Mn and Ni from the spinel LNMO into the electrolyte during cycling. Eventually, it will successfully enhance the discharge capacity and improve

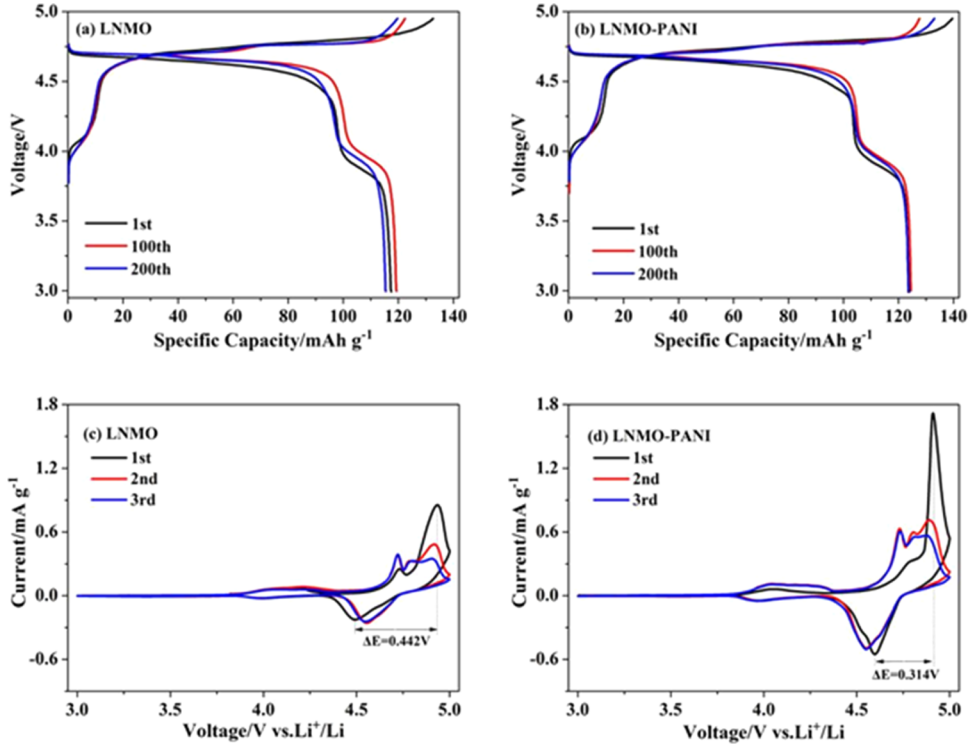

Figure 6. First, 100th, and 200th charge−discharge curves of (a) the bare LNMO, (b) the LNMO−PANI composite material electrodes at room temperature (25 °C), the cyclic voltammetry (CV) curves of (c) the bare LNMO and (d) the LNMO−PANI composite material electrodes at room temperature by a sweep rate of 0.05 mV s^{-1}.

DOI: 10.1021/acsomega.8b02571
ACS Omega 2019, 4, 185−194

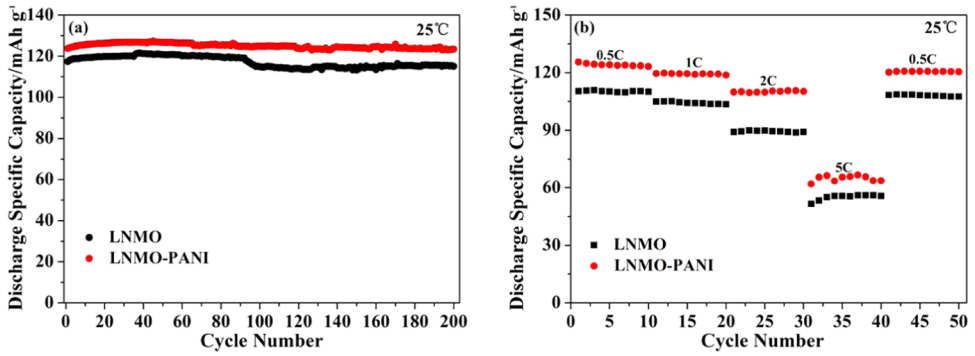

Figure 7. Cycling performance of (a) the bare LNMO and the LNMO−PANI composite material at 0.5C and room temperature and (b) the rate capabilities of the bare LNMO and the LNMO−PANI composite material electrodes at different current densities and room temperature.

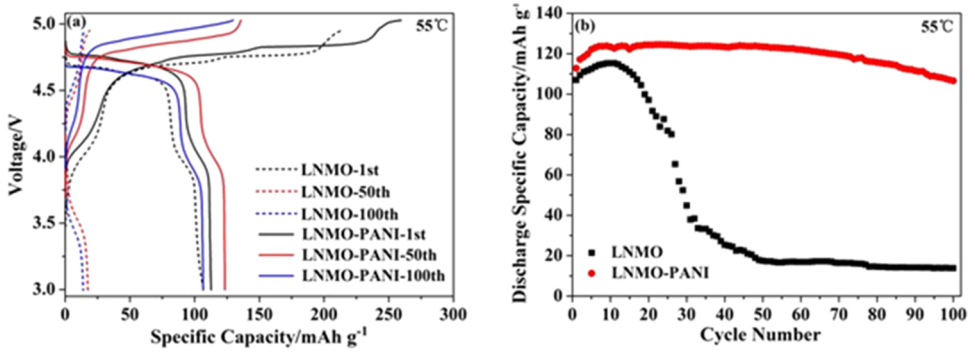

Figure 8. (a) Charge−discharge curves of the bare LNMO and the LNMO−PANI composite material electrodes, (b) cycling performance of the bare LNMO and the LNMO−PANI composite material electrodes at elevated temperature (55 °C).

the cycling stability. Figure 7b shows the rate capabilities of the bare and modified LNMO electrodes at different current densities and room temperature. The activation conditions as above, then testing at various current densities from 0.5 to 5.0C for 10 cycles each, finally returning to 0.5C for 10 cycles. The rate capacities of the bare LNMO are 110.2, 104.2, 89.8, and 55.7 mAh g^{-1} at 0.5, 1.0, 2.0, and 5.0C, respectively. When the current density was returned to 0.5C, the rate capacity recovered up to 108.3 mAh g^{-1}. In comparison, when the rate capacities of the LNMO−PANI composite material accompanied by 124.1 to 65.5 mAh g^{-1} along with the current densities changed from 0.5 to 5.0C, as well as the rate capacity rising to 120.8 mAh g^{-1} while the current density backing up to 0.5C. Thus, it can be seen that the bare LNMO exhibits a relatively poor rate capability. It indicates that the PANI layer could improve the characteristics of the LNMO, leading to an excellent rate capability at different current densities.

The charge−discharge curves of the bare LNMO and the LNMO−PANI composite material electrodes were acquired at an elevated temperature (55 °C) by the first, 50th and 100th cycles. Before cycling, the cells were activated at 0.1C for 3 cycles at room temperature. As shown in Figure 8a,b, the electrodes display the analogical initial discharge capacities of 107.0 and 112.8 mAh g^{-1}, respectively. Subsequently, the discharge capacity of the bare LNMO electrode decreases to 17.5 mAh g^{-1}. Meanwhile, the LNMO−PANI composite material rises first and then remains at 123.4 mAh g^{-1} until 50 cycles. After that, the discharge capacity of the composite electrode tardily drops to 106.6 mAh g^{-1} at the 100th cycle. Although the higher temperature can promote the transfer behavior of lithium ions and soaking of electrolyte into the separator film, it would accelerate the undesirable interfacial reactions between the cathode and the electrolyte. The products from these side reactions are easy to deposit on the surface of LNMO, resulting in the increase of the polarization resistance and interfacial impedance. In particular, at the high operating voltage of 5 V, it would also expedite the formation of HF along with the decomposition of the electrolyte. The incremental concentration of HF would enhance the dissolution of Mn and Ni, which causes a large irreversible capacity attenuation as shown in Figure 8a. By contrast, the PANI layer coated on the surfer of LNMO, working as an admirable protective skin, could significantly reduce the dissolution of Mn and Ni by suppressing the decomposition of the electrolyte to a great extent. Hence, it can be seen that the discharge capacity of the composite electrode presents a relatively satisfied reversibility as shown in Figure 8b. Figure 8c compares the cycling performances of the bare LNMO and the LNMO−PANI composite material at 0.5C and elevated temperatures. Before formally testing, the cells were activated at 0.1C for 3 cycles at room temperature. The bare LNMO delivers a discharge capacity of 13.9 mAh g^{-1} at the 100th cycle, which means that it has a capacity retention of only 13.0%. However, the discharge capacity of the LNMO−PANI composite material is 106.6 mAh g^{-1} at the 100th cycle, and it also shows a better capacity retention of 94.5% than that of the bare LNMO. The cycling performance tautologically proves that the LNMO−PANI composite material possesses more superior high temperature cycle stability than the bare LNMO. The PANI coating layer separates the electrolyte and LMNO effectively, decreases the side reaction at the highly oxidizing conditions (>4.5 V), and suppresses the dissolution of the transition metal ions.

DOI: 10.1021/acsomega.8b02571
ACS Omega 2019, 4, 185−194

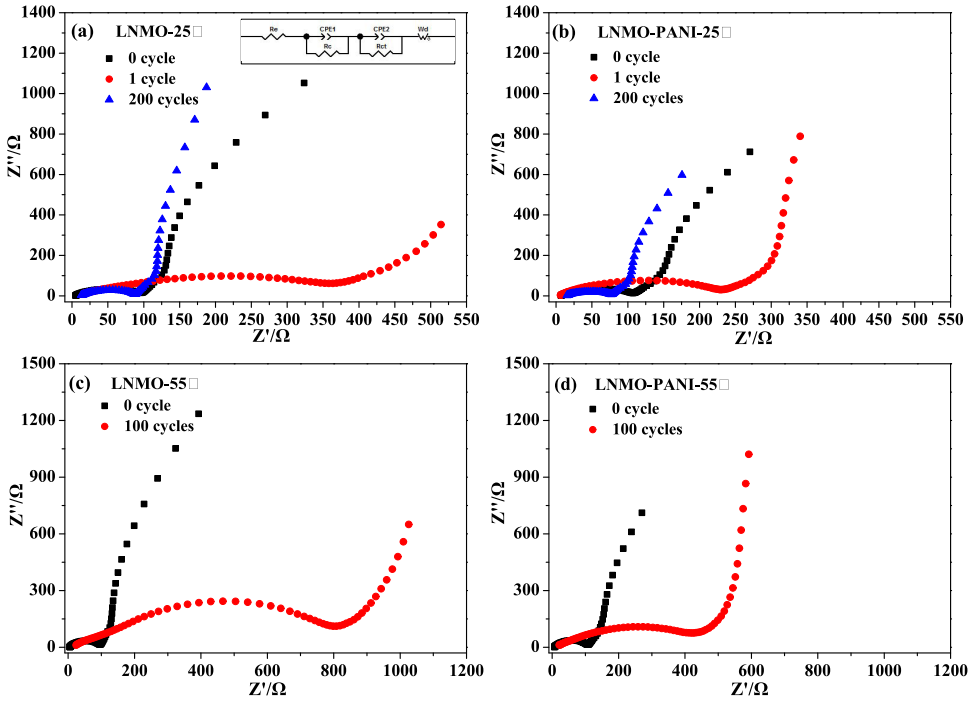

Figure 9. Nyquist plots of composite materials: (a) the bare LNMO composite material at 25 °C with the inset of the equivalent circuit; (b) the LNMO−PANI composite material at 25 °C; (c) the bare LNMO composite at 55 °C; (d) the LNMO−PANI composite material at 55 °C.

To some extent, electrochemical impedance spectroscopy (EIS) may be considered as one of the most cogent tools to study the difference of the electrochemical behaviors between the bare LNMO and the LNMO−PANI composite material electrodes.[45] In Figure 9, the Nyquist plots show an intercept at high frequency for the electrolyte resistance, R_e. R_c is marked as the contact resistance at high frequency from the intercept of the semicircle of the *x*-axis, which can be obtained from the electrical contacts between the electrolyte, the active materials, and the current collector. Following, R_{ct}, the charge transfer resistance, is located at the high-middle frequency region, and the low frequency region of the straight line is interpreted to the diffusion resistance of the lithium ions into the electrode material, which is the Warburg diffusion impedance, W_d. From Figure 9a,b, the diameters of the semicircles for the bare and coated electrodes before cycling at room temperature are 97 and 107 Ω, respectively. After the 1st cycle, a legible distinction was observed that the diameter values were 365 and 230 Ω. The diameter of the semicircle data, 90 and 78 Ω, were gained after 200 cycles, which were also used for fitting the equivalent circuit in the insets of Figure 9a. Before cycling, at elevated temperatures, alternating current impedance tests of the cells before and after coating were also executed. The Nyquist plots still consist of a semicircle and a straight line. The diameters of the semicircle values, 808 and 436 Ω, were obtained after 100 cycles at 55 °C, and they were also matched with the equivalent circuit. From Figure 9, it can be seen that there is a clear increase after coating for the conductivity at both room and elevated temperatures, which again confirms that the introduction of the PANI layer is an effective method for enhancing the electron transport of LNMO. As a consequence, the PANI layer, working as a conductive coating agent, can diminish the polarization resistance and interfacial impedance by improving the severe interfacial reactions, leading to a significant improvement in the electrochemical performance.

As we all know that the diffusion coefficient of the lithium ions in the electrode is identified as an important parameter for measuring the electrochemical performance of active materials,[46,47] and it could be calculated by eqs 4 and 5. Where Z_{re} is the real axis resistance of the low frequency region (Ω); σ_w is the Warburg diffusion impedance coefficient (Ω $s^{-0.5}$); and ω is the angular frequency at low frequency (s^{-1}); R is the gas constant (8.314 J mol^{-1} K^{-1}); T is the absolute temperature (K); n is the number of the transferred electron of per mole active material involved in the electrode reaction; A is the area of the electrode surface (cm^2); F is the Faraday's constant (96485 C mol^{-1}); and c is the molar concentration of the lithium ions (mol cm^{-3}). The plot of Z_{re} vs the reciprocal square root of the lower angular frequencies is shown in Figure 10. It is observed that the σ_w values of the LNMO−PANI composite material electrodes are lower than the bare LNMO electrodes at both room and elevated temperatures. Con-

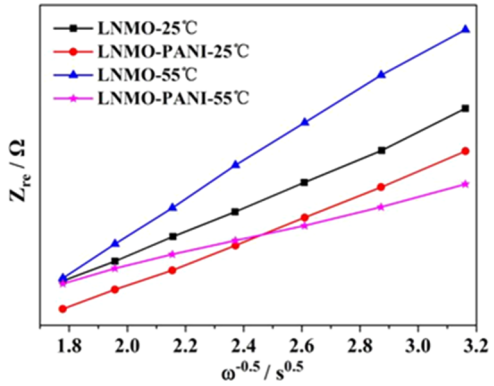

Figure 10. Plot of Z_{re} vs the reciprocal square root of the lower angular frequencies for the bare LNMO and the LNMO−PANI composite material at 25 and 55 °C.

DOI: 10.1021/acsomega.8b02571
ACS Omega 2019, 4, 185−194

sistently, the diffusion coefficient of the lithium ions for LNMO−PANI composite material electrodes is higher than that of the bare LNMO electrodes at both room and elevated temperatures. Therefore, the charge transfer reaction is stronger in the LNMO−PANI composite material electrodes than the bare LNMO electrodes. Besides, the parameter values of the bare LNMO and LNMO−PANI composite material electrodes at both 25 and 55 °C are all recorded in Table 1.

$$D_{Li^+} = \frac{R^2T^2}{2n^4A^2F^4\sigma_w^2c^2} \quad (4)$$

$$Z_{re} = R_e + R_{ct} + \sigma_w\omega^{-0.5} \quad (5)$$

Table 1. Parameter Values of the Bare LNMO and the LNMO−PANI Composite Material Electrodes at Both 25 and 55 °C

sample numbers	R_e/Ω	R_{ct}/Ω	$\sigma_w/(\Omega\ s^{-0.5})$	$D_{Li^+}/(cm^2\ s^{-1})$
LNMO-25 °C	12.33	537.0	50.16	1.27×10^{-13}
LNMO−PANI-25 °C	14.28	469.4	46.24	1.50×10^{-13}
LNMO-55 °C	16.96	909.2	73.56	5.92×10^{-14}
LNMO−PANI-55 °C	13.27	502.4	28.37	3.98×10^{-13}

The cells after 200 cycles at 25 °C and after 100 cycles at 55 °C were disassembled. Then the sheets, the separator films, the Li foils, and the electro-conductive gaskets were all dissolved in the dimethyl carbonate (DMC) along with the anode and cathode shells. Afterwards, they were placed for 2 days in the Ar-filled glove-box. Next, inductively coupled plasma (ICP) was used to observe the dissolved amount of Ni and Mn from the spinel LNMO into the electrolyte, recorded in Table 2. It is

Table 2. Dissolution Amount of Ni and Mn for the Bare LNMO and LNMO−PANI Composite Material Cells After 200 Cycles at 25 °C and After 100 Cycles at 55 °C

sample numbers	Ni/μg	Mn/μg
LNMO- 25 °C	30.7	21.4
LNMO−PANI-25 °C	23.9	16.0
LNMO-55 °C	67.5	40.1
LNMO−PANI-55 °C	29.1	20.5

clear to observe that the dissolution amount of Ni and Mn of the bare LNMO is greater than the LNMO−PANI composite material, which again demonstrates that the PANI layer, working as a protective skin, effectively suppresses the dissolution of the transition metal ions.

Figure 11a−f shows the EDS mappings of LNMO−PANI electrode. In Figure 11c, the presence of N element indicates that the PANI is still coated on the surface of the LNMO material after cycling, which plays a protective layer on the LNMO. The homogeneous distribution of N, Mn, and Ni elements is illustrated in Figure 11g−i. The binding energy of N 1s spectra is 399.8 eV, indicating that the coated PANI layer still exists, working as an admirable protective skin. Meanwhile, it showed that the Mn 2p and Ni 2p bands are mainly located at 653.4, 642.5, 641.1, and 858.8 eV (satellite peak), 854.2 eV, respectively, which is consistent with the previous literature.[17]

Therefore, it is believed that the conductive PANI coating on the surface of the LNMO particles can not only act as an electron-conductive layer, but can also be used as a primary protective barrier to confront the decomposition of the electrolyte. The possible schematic illustration of how the PANI layer works as an effective protective layer to suppress the detrimental electrolyte decomposition and reduce the dissolution of Mn is shown in Figure 12.[33]

CONCLUSIONS

An innovative way to improve the electrochemical performance of LNMO by coating the relatively homogeneous PANI layer has been successfully implemented. It is proved that the LNMO−PANI composite material shows a higher capacity retention and a better rate capability at room and elevated temperatures than that of the bare LNMO. The promising electrochemical performance of the LNMO−PANI composite material can be ascribed to three reasons: (1) the polymer PANI, working as a conductive coating agent, can enhance the conductivity of the bare LNMO; (2) the PANI layer can also diminish the polarization resistance and interfacial impedance by improving the severe interfacial reactions; (3) the external PANI layer on the LNMO particles, using as a protective skin, can relieve the serious decomposition of the electrolyte in the highly oxidizing (>4.5 V) and elevated temperature environment, thus suppressing the dissolution of transition metal ions into the electrolyte. This work established a method to relieve ion dissolution in other similar cathode materials. In consideration of the superior electrochemical performance with the PANI coating, we believe that the LNMO−PANI composite material is likely to be a high-energy and high-power cathode material for the lithium-ion battery.

EXPERIMENTAL SECTION

Preparation of the LNMO−PANI Composite Material. A certain amount of the LNMO powder (WUJIE SCIENCE & TECHNOLOGY CO., LTD) was added into distilled water and stirred for 1 h. Then 10 mL of 1 mol/L HCl solution was prepared and added into the aqueous solution. When the mixed solution was precooled in a 0 °C ice-water bath for 20 min, 5.1 wt % of aniline (Sinopharm Chemical Reagent Limited Corporation, SCRC) was slowly dripped into the solution and stirred for 20 min. Afterwards, 11.5 mL of 1 mol/L ammonium peroxydisulfate was slowly added into the above reacting aqueous solution with continuous stirring for 20 h and the reaction temperature was always kept at 0 °C. After that, the coated nanoparticles were washed repeatedly with a large amount of distilled water and ethanol until the filtrate was colorless by the suction filter. Finally, the wet LNMO−PANI composite material was dried in a vacuum oven at 80 °C for 12 h in Figure 13.

Physical Characterization. The presence of PANI in the composite was confirmed by a Raman spectrometer (LabRAM HR Evolution, HORIBA JOBIN YVON) with 632.8 nm laser excitation. The PANI content in the composite was determined by thermogravimetric analysis (TGA, STA449F3, NETZSCH). The morphologies of the samples were characterized by field emission-scanning electron microscopy (FE-SEM, SU-8010, HITACHI) equipped with energy dispersive spectroscopy (EDS). To correctly measure the thickness of the PANI layer, Transmission electron microscopy (TEM, JEM-2100, JEOL) was performed operating at 200 kV. The crystal structure analyses of the as-prepared composite electrode and the bare LNMO electrode were determined by X-ray powder diffraction (XRD, D8 ADVANCE, BRUKER) with a Cu Kα radiation.

DOI: 10.1021/acsomega.8b02571
ACS Omega 2019, 4, 185−194

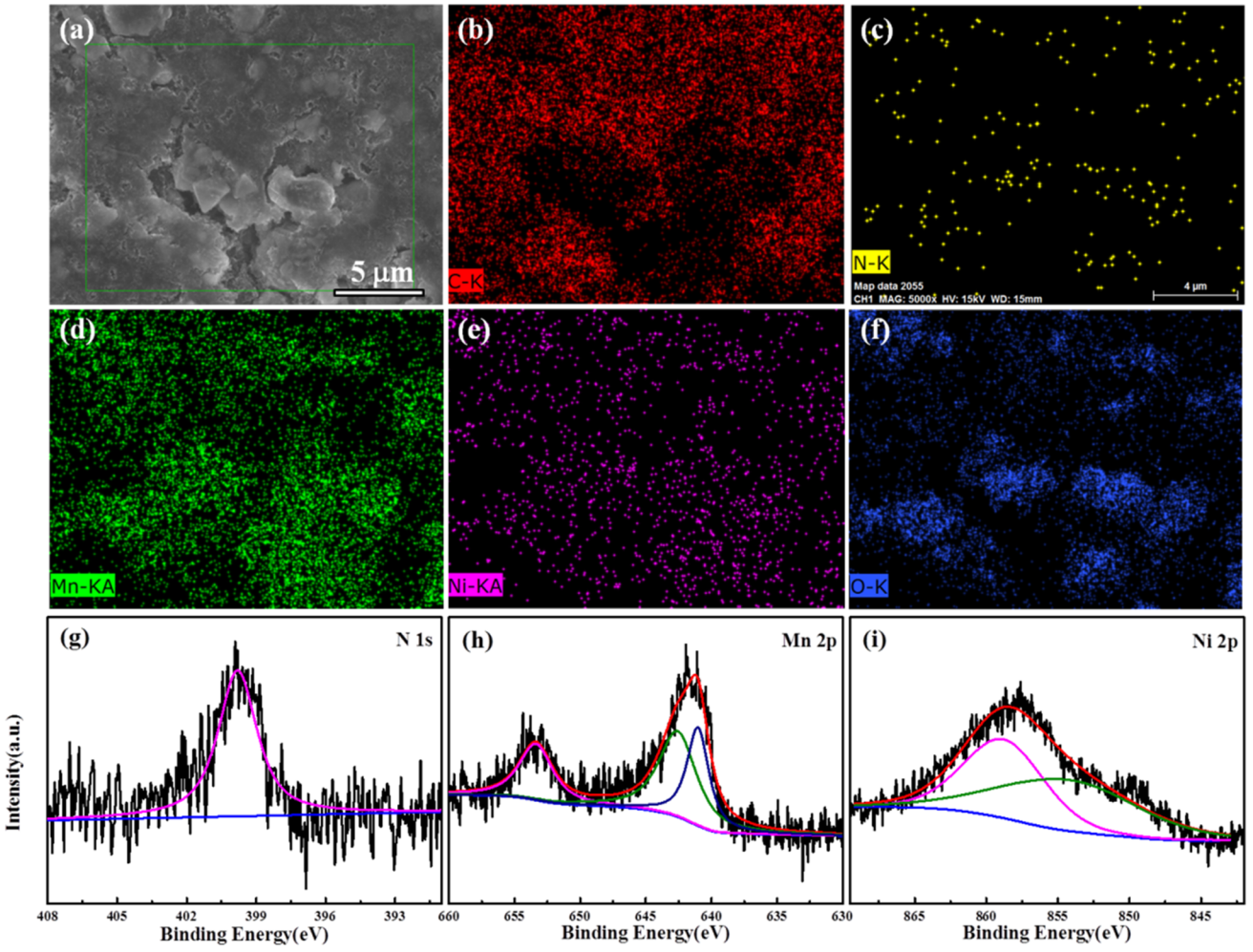

Figure 11. EDS mapping (a–f) and the X-ray photoelectron spectroscopy results (g–i) of the LNMO–PANI composite electrode after 200 cycles.

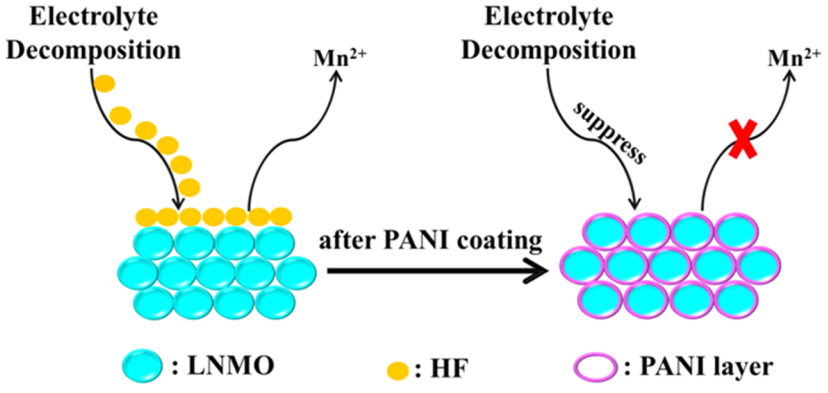

Figure 12. Schematic illustration of the mechanism that PANI layer works as an effective protective layer to suppress the detrimental electrolyte decomposition and reduce the dissolution of Mn.

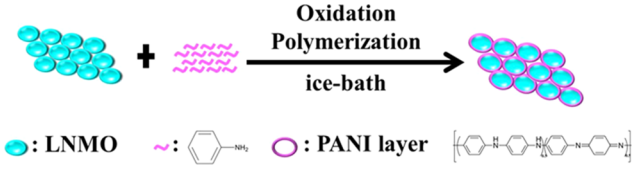

Figure 13. Schematic of the preparation process with LNMO and aniline by the in situ chemical oxidation polymerization method.

Electrochemical Measurements. The electrochemical performances of the materials were evaluated via CR2032 coin cells. A mixture of 80 wt % active materials and 10 wt % conductive agent (Super P) with 10 wt % poly(vinylidene fluoride) in *N*-methyl-2-pyrrolidone solvent was ground into slurry, and then the slurry was pasted on Al foil. Subsequently, under vacuum at 60 °C overnight, the CR2032 coin cells were assembled in an Ar-filled glove-box using Li foil as the counter electrode, the Whatman glass fiber film as the separator, and 1 M $LiPF_6$ dissolved in ethylene carbonate and DMC (v/v =

DOI: 10.1021/acsomega.8b02571
ACS Omega 2019, 4, 185–194

1:1) as the electrolyte. The cycling performance test was carried out between 3.0 and 4.95 V at both room (25 °C) and elevated temperatures (55 °C) by the LAND test system (CT2001A, Wuhan, China). Rate capability was also performed on the same instrument and under same conditions. The cyclic voltammetry (CV) experiment was accomplished using the electrochemical workstation (CHI 760E, Shanghai, China) at a scan rate of 0.05 mV s^{-1}. Electrochemical impedance spectroscopy (EIS) was conducted on the electrochemical workstation (CHI 760E, Shanghai, China) with a frequency range from 0.1 HZ to 100 kHz. Inductively coupled plasma (ICP, ELAN DRC-e, PerkinElmer) was operated to observe the dissolved amount of Ni and Mn from the spinel LNMO into the electrolyte.

AUTHOR INFORMATION

Corresponding Authors

*E-mail: wd_chem@163.com (D.W.).
*E-mail: shutingyang@foxmail.com (S.Y.).

ORCID

Hongyu Dong: 0000-0002-9878-3626
Shuting Yang: 0000-0001-7841-0016

Notes

The authors declare no competing financial interest.

ACKNOWLEDGMENTS

This work was supported by the key Science and Technology Foundation of Henan Province (142102210452, 172102210349, and 142300410166). The support from the Fund of Department of Education of Henan Province (14B150006, 15A150057) and the National Natural Science Foundation of China (51502082).

REFERENCES

(1) Marom, R.; Amalraj, S. F.; Leifer, N.; Jacob, D.; Aurbach, D. A review of advanced and practical lithium battery materials. *J. Mater. Chem.* **2011**, *21*, 9938−9954.

(2) Tarascon, J. M. Key challenges in future Li-battery research. *Philos. Trans. R. Soc., A* **2010**, *368*, 3227−3241.

(3) Xie, Z. Q.; Eikhuemelo, H.; Zhao, J. Q.; Cain, C.; Xu, W. W.; Wang, Y. Ni and Fe dual-doped Li4Mn5O12 spinels as cathode materials for high-voltage Li-ion batteries. *J. Electrochem. Soc* **2015**, *162*, A1523−A1529.

(4) Caballero, A.; Hernán, L.; Melero, M.; Morales, J.; Moreno, R.; Ferrari, B. LiNi0.5Mn1.5O4 thick-film electrodes prepared by electrophoretic deposition for use in high voltage lithium-ion batteries. *J. Power Sources* **2006**, *158*, 583−590.

(5) Chen, Y. Y.; Sun, Y.; Huang, X. J. Origin of the Ni/Mn ordering in high-voltage spinel LiNi0.5Mn1.5O4: the role of oxygen vacancies and cation doping. *Comput. Mater. Sci.* **2016**, *115*, 109−116.

(6) Hong, S. K.; Mho, S. I.; Yeo, I. H.; Kang, Y. K.; Kim, D. W. Structural and electrochemical characteristics of morphology-controlled Li[Ni0.5Mn1.5]O4 cathodes. *Electrochim. Acta* **2015**, *156*, 29−37.

(7) Luo, W. B. Effect of morphology on the physical and electrochemical properties of the high-voltage spinel cathode LiMn1.5Ni0.5O4. *J. Alloys Compd.* **2015**, *636*, 24−28.

(8) Shiiba, H.; Zettsu, N.; Nakayama, M.; Oishi, S.; Teshima, K. Defect formation energy in spinel LiNi0.5Mn1.5O4-δ using Ab initio DFT calculations. *J. Phys. Chem. C* **2015**, *119*, 9117−9124.

(9) Liu, G. Q.; Wen, L.; Liu, Y. M. Spinel LiNi0.5Mn1.5O4 and its derivatives as cathodes for high-voltage Li-ion batteries. *J. Solid State Electrochem.* **2010**, *14*, 2191−2202.

(10) Nayak, P. K.; Levi, E.; Grinblat, J.; Levi, M.; Markovsky, B.; Munichandraiah, N.; Sun, Y. K.; Aurbach, D. High-capacity layered-spinel cathodes for Li-ion batteries. *ChemSusChem* **2016**, *9*, 2404−2413.

(11) Goodenough, J. B.; Kim, Y. Challenges for rechargeable Li batteries. *Chem. Mater.* **2010**, *22*, 587−603.

(12) Lu, D. P.; Tao, J. H.; Yan, P. F.; Henderson, W. A.; Li, Q. Y.; Shao, Y. Y.; Helm, M. L.; Borodin, O.; Graff, G. L.; Polzin, B.; Wang, C. M.; Engelhard, M.; Zhang, J. G.; De Yoreo, J. J.; Liu, J.; Xiao, J. Formation of Reversible Solid Electrolyte Interface on Graphite Surface from Concentrated Electrolytes. *Nano Lett.* **2017**, *17*, 1602−1609.

(13) Steinhauer, M.; Risse, S.; Wagner, N.; Friedrich, K. A. Investigation of the Solid Electrolyte Interphase Formation at Graphite Anodes in Lithium-Ion Batteries with Electrochemical Impedance Spectroscopy. *Electrochim. Acta* **2017**, *228*, 652−658.

(14) Xu, J. J.; Xia, Q. B.; Chen, F. Y.; Liu, T.; Li, L.; Cheng, X. Y.; Lu, W.; Wu, X. D. Facilely solving cathode/electrolyte interfacial issue for high-voltage lithium ion batteries by constructing an effective solid electrolyte interface film. *Electrochim. Acta* **2016**, *191*, 687−694.

(15) Song, M. S.; Kim, D. S.; Park, E.; Choi, J. M.; Kim, H. Simultaneous fluorination of active material and conductive agent for improving the electrochemical performance of LiNi0.5Mn1.5O4 electrode for lithium-ion batteries. *J. Power Sources* **2016**, *326*, 156−161.

(16) Pieczonka, N. P. W.; Liu, Z. Y.; Lu, P.; Olson, K. L.; Moote, J.; Powell, B. R.; Kim, J. H. Understanding transition-metal dissolution behavior in LiNi0.5Mn1.5O4 high-voltage spinel for lithium ion batteries. *J. Phys. Chem. C* **2013**, *117*, 15947−15957.

(17) Deng, Y.; Mou, J.; He, L.; Xie, F.; Zheng, Q.; Xu, C.; Lin, D. A core-shell structured LiNi0.5Mn1.5O4@LiCoO2 cathode material with superior rate capability and cycling performance. *Dalton Trans.* **2018**, *47*, 367−375.

(18) Mou, J.; Deng, Y.; He, L.; Zheng, Q.; Jiang, N.; Lin, D. Critical roles of semi-conductive LaFeO3 coating in enhancing cycling stability and rate capability of 5 V LiNi0.5Mn1.5O4 cathode materials. *Electrochim. Acta* **2018**, *260*, 101−111.

(19) Lu, J.; Chang, Y. L.; Song, B. H.; Xia, H.; Yang, J. R.; Lee, K. S.; Lu, L. High energy spinel-structured cathode stabilized by layered materials for advanced lithium-ion batteries. *J. Power Sources* **2014**, *271*, 604−613.

(20) Mun, J.; Yim, T.; Park, K.; Ryu, J. H.; Kim, Y. G.; Oh, S. M. Surface film formation on LiNi0.5Mn1.5O4 electrode in an ionic liquid solvent at elevated temperature. *J. Electrochem. Soc.* **2011**, *158*, A453−A457.

(21) Kim, J. W.; Kim, D. H.; Oh, D. Y.; Lee, H.; Kim, J. H.; Lee, J. H.; Jung, Y. S. Surface chemistry of LiNi0.5Mn1.5O4 particles coated by Al2O3 using atomic layer deposition for lithium-ion batteries. *J. Power Sources* **2015**, *274*, 1254−1262.

(22) Sun, H. D.; Xia, B. B.; Liu, W. W.; Fang, G. Q.; Wu, J. J.; Wang, H. B.; Zhang, R. X.; Kaneko, S.; Zheng, J. W.; Wang, H. Y.; Li, D. C. Significant improvement in performances of LiNi0.5Mn1.5O4 through surface modification with high ordered Al-doped ZnO electro-conductive layer. *Appl. Surf. Sci.* **2015**, *331*, 309−314.

(23) Rajammal, K.; Sivakumar, D.; Duraisamy, N.; Ramesh, K.; Ramesh, S. Enhanced electrochemical properties of ZnO-coated LiMnPO4 cathode materials for lithium ion batteries. *Ionics* **2016**, *22*, 1551−1556.

(24) Brutti, S.; Gentili, V.; Reale, P.; Carbone, L.; Panero, S. Mitigation of the irreversible capacity and electrolyte decomposition in a LiNi0.5Mn1.5O4/nano-TiO2 Li-ion battery. *J. Power Sources* **2011**, *196*, 9792−9799.

(25) Wang, G.; Wen, W. C.; Chen, S. H.; Yu, R. Z.; Wang, X. Y.; Yang, X. K. Improving the electrochemical performances of spherical LiNi0.5Mn1.5O4 by Fe2O3 surface coating for lithium-ion batteries. *Electrochim. Acta* **2016**, *212*, 791−799.

(26) Deng, Y.; He, L.; Ren, J.; Zheng, Q.; Xu, C.; Lin, D. Reinforcing cycling stability and rate capability of LiNi 0.5 Mn 1.5 O 4 cathode by dual-modification of coating and doping of a fast-ion conductor. *Mater. Res. Bull.* **2018**, *100*, 333−344.

DOI: 10.1021/acsomega.8b02571
ACS Omega 2019, 4, 185−194

(27) Mou, J.; Deng, Y.; Song, Z.; Zheng, Q.; Lam, K. H.; Lin, D. Excellent rate capability and cycling stability in Li(+)-conductive Li2SnO3-coated LiNi0.5Mn1.5O4 cathode materials for lithium-ion batteries. *Dalton Trans.* **2018**, *47*, 7020−7028.
(28) Jin, Y. Z.; Lv, Y. Z.; Xue, Y.; Wu, J.; Zhang, X. G.; Wang, Z. B. Improved electrochemical performance of LiNi0.4Ti0.1Mn1.5O4 as cathode of lithium ion battery by carbon-coating. *RSC Adv.* **2014**, *4*, 57041−57047.
(29) Niketic, S.; Couillard, M.; MacNeil, D.; Abu-Lebdeh, Y. Improving the performance of high voltage LiMn1.5Ni0.5O4 cathode material by carbon coating. *J. Power Sources* **2014**, *271*, 285−290.
(30) Wang, H. L.; Shi, Z. Q.; Li, J. W.; Yang, S.; Ren, R. B.; Cui, J. Y.; Xiao, J. L.; Zhang, B. Direct carbon coating at high temperature on LiNi0.5Mn1.5O4 cathode: unexpected influence on crystal structure and electrochemical performances. *J. Power Sources* **2015**, *288*, 206−213.
(31) Xue, L.; Liao, Y.; Yang, L.; Li, X.; Li, W. Improved rate performance of LiNi0.5Mn1.5O4 cathode for lithium ion battery by carbon coating. *Ionics* **2015**, *21*, 1269−1275.
(32) Kim, M. C.; Kim, S. H.; Aravindan, V.; Kim, W. S.; Lee, S. Y.; Lee, Y. S. Ultrathin polyimide coating for a spinel LiNi0.5Mn1.5O4 cathode and its superior lithium storage properties under elevated temperature conditions. *J. Electrochem. Soc.* **2013**, *160*, A1003−A1008.
(33) Gao, X. W.; Deng, Y. F.; Wexler, D.; Chen, G. H.; Chou, S. L.; Liu, H. K.; Shi, Z. C.; Wang, J. Z. Improving the electrochemical performance of the LiNi0.5Mn1.5O4 spinel by polypyrrole coating as a cathode material for the lithium-ion battery. *J. Mater. Chem. A* **2015**, *3*, 404−411.
(34) Kapil, A.; Taunk, M.; Chand, S. Preparation and charge transport studies of chemically synthesized polyaniline. *J. Mater. Sci.: Mater. Electron.* **2010**, *21*, 399−404.
(35) Khan, A.; Aldwayyan, A. S.; Alhoshan, M.; Alsalhi, M. Synthesis by in situ chemical oxidative polymerization and characterization of polyaniline/iron oxide nanoparticle composite. *Polym. Int.* **2010**, *59*, 1690−1694.
(36) Wu, F.; Chen, J. Z.; Li, L.; Zhao, T.; Chen, R. J. Improvement of rate and cycle performence by rapid polyaniline coating of a MWCNT/sulfur cathode. *J. Phys. Chem. C* **2011**, *115*, 24411−24417.
(37) Xue, Q. R.; Li, J. L.; Xu, G. F.; Zhou, H. W.; Wang, X. D.; Kang, F. Y. In situ polyaniline modified cathode material Li-[Li0.2Mn0.54Ni0.13Co0.13]O2 with high rate capacity for lithium ion batteries. *J. Mater. Chem. A* **2014**, *2*, 18613−18623.
(38) Zengin, H.; Erkan, B. Synthesis and characterization of polyaniline/silicon dioxide composites and preparation of conductive films. *Polym. Adv. Technol.* **2010**, *21*, 216−223.
(39) Julien, C. M.; Massot, M. Lattice vibrations of materials for lithium rechargeable batteries I. lithium manganese oxide spinel. *Mater. Sci. Eng., B* **2003**, *97*, 217−230.
(40) Oh, S. H.; Chung, K. Y.; Jeon, S. H.; Kim, C. S.; Cho, W. I.; Cho, B. W. Structural and electrochemical investigations on the LiNi0.5−xMn1.5−yMx+yO4 (M = Cr, Al, Zr) compound for 5 V cathode material. *J. Alloys Compd.* **2009**, *469*, 244−250.
(41) Ghanbari, K.; Moloudi, M. Flower-like ZnO decorated polyaniline/reduced graphene oxide nanocomposites for simultaneous determination of dopamine and uric acid. *Anal. Biochem.* **2016**, *512*, 91−102.
(42) de Oliveira, L. R.; Manzato, L.; Mascarenhas, Y. P.; Sanches, E. A. The influence of heat treatment on the semi-crystalline structure of polyaniline emeraldine-salt form. *J. Mol. Struct.* **2017**, *1128*, 707−717.
(43) Goswami, M.; Mukherjee, A.; Ghosh, R.; Basu, S.; Meikap, A. K. Enhanced magnetoconductivity and electrical property of MWCNT-CdS nanocomposite embedded in polyaniline. *Solid State Sci.* **2016**, *60*, 37−44.
(44) Liu, D. Q.; Lu, Y. H.; Goodenough, J. B. Rate properties and elevated-temperature performances of LiNi 0.5−xCr2xMn1.5−xO4 (0 ≤ 2x ≤ 0.8) as 5 V cathode materials for lithium-ion batteries. *J. Electrochem. Soc* **2010**, *157*, A1269−A1273.
(45) Cao, J. C.; Xiao, K.; Jiang, F.; Xi, X. M.; Liao, D. Q.; He, D. Surface design with spinel LiMn1.5Ni0.5O4 for improving electrochemical properties of LiNi0.5Co0.2Mn0.3O2 at high cut-off voltage. *Mater. Lett.* **2016**, *184*, 29−33.
(46) Shenouda, A. Y.; Liu, H. K. Electrochemical behaviour of tin borophosphate negative electrodes for energy storage systems. *J. Power Sources* **2008**, *185*, 1386−1391.
(47) Shenouda, A. Y.; Liu, H. K. Studies on electrochemical behaviour of zinc-doped LiFePO4 for lithium battery positive electrode. *J. Alloys Compd.* **2009**, *477*, 498−503.

DOI: 10.1021/acsomega.8b02571
ACS Omega 2019, 4, 185−194